Journal of Power Sources 268 (2014) 787–793

Contents lists available at ScienceDirect

Journal of Power Sources

journal homepage: www.elsevier.com/locate/jpowsour

Aluminum oxide as a dual-functional modifier of Ni-based anodes of solid oxide fuel cells for operation on simulated biogas

Feng Wang [a], Wei Wang [b], Ran Ran [a], Moses O. Tade [b], Zongping Shao [a, b, *]

[a] State Key Laboratory of Materials-Oriented Chemical Engineering, College of Chemistry & Chemical Engineering, Nanjing University of Technology, Nanjing 210009, China
[b] Department of Chemical Engineering, Curtin University, Perth, WA 6458, Australia

HIGHLIGHTS

- Al_2O_3 and SnO_2 additives are introduced into the Ni–YSZ cermet anode.
- The addition of the modifier could increase the coking resistance towards methane.
- Al_2O_3 had a positive effect on cell performance while SnO_2 had a negative effect.
- High power output of 571 mW cm^{-2} was obtained with biogas as fuel at 850 °C.
- The fuel cell with Al_2O_3 modified Ni–YSZ anode delivered good stability.

ARTICLE INFO

Article history:
Received 31 March 2014
Received in revised form
14 June 2014
Accepted 16 June 2014
Available online 24 June 2014

Keywords:
Solid-oxide fuel cells
Anode
Biogas
Carbon deposition
Oxide modification

ABSTRACT

Al_2O_3 and SnO_2 additives are introduced into the Ni–YSZ cermet anode of solid oxide fuel cells (SOFCs) for operation on simulated biogas. The effects of incorporating Al_2O_3/SnO_2 on the electrical conductivity, morphology, coking resistance and catalytic activity for biogas reforming of the cermet anode are systematically studied. The electrochemical performance of the internal reforming SOFC is enhanced by introducing an appropriate amount of Al_2O_3 into the anode, but it becomes worse with excess alumina addition. For SnO_2, a negative effect on the electrochemical performance is demonstrated, although the coking resistance of the anode is improved. For fuel cells operating on biogas, stable operation under a polarization current for 130 h at 750 °C is achieved for a cell with an Al_2O_3-modified anode, while cells with unmodified or SnO_2-modified Ni–YSZ anodes show much poorer stability under the same conditions. The improved performance of the cell with the Al_2O_3-modified anode mainly results from the suppressed coking and sintering of the anode and from the formation of $NiAl_2O_4$ in the unreduced anode. In sum, modifying the anode with Al_2O_3 may be a useful and facile way to improve the coking resistance and electrochemical performance of the nickel-based cermet anodes for SOFCs.

1. Introduction

Due to the rapid consumption of fossil fuels and the increased awareness of global warming and environmental pollution, there is increasing interest in the search for innovative energy conversion technologies that are more sustainable and efficient than the current power generation technology based on combustion. Fuel cells are a type of such technology, and they enable efficient and clean conversion of chemical energy in fuels directly into electrical power via electrochemical means. Among the various types of fuel cells, solid oxide fuel cells (SOFCs) have recently received particular attention because of their high energy conversion efficiency, low emissions, fuel flexibility and high quality of exhaust heat. SOFCs apply non-precious metal electrode catalysts and solid electrolytes, providing great potential for relatively low manufacturing costs and facile operation. Due to the high operation temperature of SOFCs, in addition to hydrogen, a wide range of chemicals could directly be used as the fuels [1–5].

Additionally, energy conversion systems with carbon-neutral and zero-emission features could be constructed using biomass as the fuel [6,7]. Biogas, a mixture of CH_4, CO_2 and trace impurities, is an important biomass-derived fuel. Currently, most biogas produced at landfill sites is wastefully vented into the atmosphere,

* Corresponding author. State Key Laboratory of Materials-Oriented Chemical Engineering, College of Chemistry & Chemical Engineering, Nanjing University of Technology, Nanjing 210009, China. Tel.: +86 25 83172256; fax: +86 25 83172242.
E-mail address: shaozp@njtech.edu.cn (Z. Shao).

http://dx.doi.org/10.1016/j.jpowsour.2014.06.087
0378-7753/

significantly contributing to greenhouse gas emissions. The utilization of biogas for electricity production is currently an underexploited opportunity to diversify our chemical and energy sources, lessen our dependence on fossil fuels and lower greenhouse gas emissions. SOFCs can operate directly on biogas because the internal reforming of biogas to syngas (a mixture of hydrogen and carbon monoxide) over the anode is possible due to the high operating temperatures. Recently, a 100 kW SOFC system fed by biogas has been proposed with a higher overall efficiency than traditional power generation systems [8]. Remarkable performance was obtained in biogas even with a CO_2-to-methane ratio as high as 1.7 [9]. This result further suggests that biogas with a relatively lower CH_4 concentration could be used as the fuel for SOFCs.

Unfortunately, the state-of-the-art SOFCs with Ni-based cermet anodes suffer from serious carbon deposition when operating on carbon-containing fuels, including biogas, because carbon formation on the anode materials is thermodynamically favored and well catalyzed by nickel [10,11]. Until now, only a few reports regarding SOFCs running on biogas through internal reforming have been available [12–14]. For example, Staniforth and Kendall have reported some results of direct-feeding of CH_4-rich landfill biogas with a short-term stability of only 6.5 h at 850 °C [12]. Tremendous efforts were devoted to the development of non-nickel anodes with improved coking resistance. However, those materials displayed decreased electrochemical activity for hydrocarbon oxidation and reduced carbon deposition rate; as a result, relatively low power output was often observed [15,16]. Thus, Ni-based cermets are still the best choice as materials for SOFC anodes due to their favorable electrochemical activity, high conductivity, easy fabrication and good thermal and chemical compatibility with the electrolyte. The coke formation problem may be reduced by incorporating a proper catalyst, such as Au, Pd or Ru, into the nickel-based cermet anode to shift it from the coke-formation region to the non-coke-formation region. Recently, Ni-based anodes with non-precious metal additives, such as SrO, BaO, La_2O_3 and CaO, have also been extensively investigated as cost-effective and highly active promoters for Ni-based cermet anodes [17–19].

Although the strategy of introducing an additional oxide appears to be promising, the effects of the secondary oxide phase require more in-depth examination, particularly in terms of phase composition, electrical conductivity, microstructure, sintering capability and operational stability. Among the various parameters, long-term stability is considered to be the most important factor for evaluating the performance of oxide-promoted Ni-based anodes. It has been reported that the Ni–YSZ cermet anode is degraded because of the sintering of the nickel particles during high temperature operation [20]. According to the literature, tin oxide and alumina were used as sintering inhibitors to prevent the aggregation of Ni to increase long-term stability [21,22]. However, there are some controversies regarding the efficiency of Sn addition to improve the coking resistance and operational stability and the efficiency of alumina addition for the improvement in coking resistance was not well realized until now.

In this work, Al_2O_3 and SnO_2 were applied as additives to Ni–YSZ anodes for SOFCs operating on biogas. Their effects on the electrochemical performance and coking resistance of the fuel cells were specifically investigated. The alumina was found to act as a sintering inhibitor and as a reactant with NiO to form a $NiAl_2O_4$ spinel structure to enhance the coking resistance of the Ni–YSZ anode in biogas. The amount of alumina was carefully controlled based on the properties of electrical conductivity, coking resistance, catalytic activity, morphology and power output. For comparison, the widely used tin oxide-promoted Ni-based anode was investigated similarly.

2. Experimental

2.1. Synthesis and fabrication

The composite anode powders were prepared by hand grinding the NiO, $(Y_2O_3)_{0.1}(ZrO_2)_{0.9}$ (YSZ) and oxide catalysts. The amount of SnO_2 in the tin oxide-modified anode was set at 2.68 wt.% of the total electrode material and the anode was labeled as Ni–YSZ–2.68Sn. This specific amount of SnO_2 was the highest reported in the literature [22,23]. In addition, two different Al_2O_3 contents (2.68 wt.% and 10 wt.%) were attempted as additives for the Ni–YSZ anode, and the corresponding anodes were labeled as Ni–YSZ–2.68Al and Ni–YSZ–10Al.

The fuel cell materials included an EDTA–citrate complexing sol–gel process, a prepared $La_{0.8}Sr_{0.2}MnO_3$ (LSM)–YSZ composite cathode [24], YSZ electrolyte and various unreduced anodes. The weight ratio of NiO to YSZ in the unreduced anodes was fixed at 3:2. In this study, the fuel cells were based on an anode-supported configuration with a thin-film YSZ electrolyte and were fabricated by a dual dry-pressing/sintering process [24]. The dual layer cells were then sintered at 1400 °C in air for 5 h to densify the electrolyte layer. The cathode layer was deposited on the cell by spraying and then calcined at 1000 °C for 5 h in air.

2.2. Catalytic activity evaluation

The catalytic activity of the various anodes for the CO_2 reforming of methane was evaluated in a flow-through fixed-bed quartz-tube reactor with an inner diameter of approximately 8 mm. For a typical test, approximately 0.2 g of anode particles in the size range of 40–60 mesh was placed in the middle of the reactor. The effluent gases from the reactor were delivered to a gas chromatograph (Varian 3800) for compositional analysis. All the anode particles were first reduced by hydrogen at 850 °C for 30 min and the reaction was conducted at 550–850 °C. The flow rate of the simulated biogas was 10 mL min^{-1} [STP] during the measurements. In this study, the simulated biogas was composed of 52.2% CH_4, 46.3% CO_2 and 1.5% N_2. The conversion of methane (X_1 (%)) during CO_2 reforming was calculated according to Eq. (1), and the conversion of CO_2 (X_2 (%)) was calculated according to Eq. (2).

$$X_1(\%) = \frac{0.5[CO]}{0.5[CO] + [CH_4]} \times 100\% \quad [1]$$

$$X_2(\%) = \frac{0.5[CO]}{0.5[CO] + [CO_2]} \times 100\% \quad [2]$$

2.3. Characterizations

In the carbon deposition tests, approximately 0.2 g of reduced anode particles was placed in a flow-through quartz-tube reactor and treated with biogas at a flow rate of 40 mL min^{-1} [STP] at 750 °C for 30 min to allow coke to form over the anode. The reactor was cooled to room temperature under helium. The deposited carbon in the treated anode was analyzed by oxygen temperature-programmed oxidation (O_2-TPO) combined with an online mass spectrometer (Hiden QIC-20) to monitor CO_2 [25].

The electrical conductivities of the various anodes were measured using the four-probe DC method. The various anode powders were first pressed into bars and sintered at 1400 °C for 5 h in static air; then two silver wires acting as the current leads and the other two silver wires as the voltage probes were attached to the bar. A constant current was created across the two current

wires and the voltage response of the two voltage probes was recorded by a source meter. The bar-shaped pellets were reduced in the same H_2–Ar atmosphere at 900 °C for 1 h and the measurements were performed from 900 to 300 °C at a cooling rate of 5 °C min^{-1} in 10 vol. % H_2–Ar atmospheres.

The phase structures of the various samples were examined using an X-ray diffractometer (XRD, Bruker D8 Advance) employing Cu Kα radiation ($\lambda = 0.1541$ nm). A scanning electron microscope (ESEM, S3400) and a field emission scanning electron microscope (FESEM, JEOL-S4800) were used to examine the morphologies of the fuel cells. Transmission electron microscopy (TEM, JEOL JEM-200CX) was also applied to characterize the electrode materials. The *I–V* and *I–P* polarization curves of the fuel cells measured at 700–850 °C were obtained using a Keithley 2420 source meter in the four-probe mode. During the measurements, ambient air served as the source of oxygen and the flow rates of hydrogen and biogas fuels were maintained at 80 mL min^{-1} [STP]. The electrochemical impedance spectroscopy (EIS) was determined by using a Solartron 1260 frequency response analyzer in combination with a Solartron 1287 potentiostat. The frequencies used for the EIS measurements ranged from 0.1 to 1000 kHz for signal amplitude of 20 mV.

3. Results and discussion

3.1. Basic properties

The XRD patterns of the various unreduced anodes (SnO_2/Al_2O_3 incorporated or pristine) after sintering at 1400 °C in air for 5 h are shown in Fig. 1a. The diffraction peaks at 2θ values of 31.5°, 45.0° and 65.6° in the XRD patterns of the two alumina-containing samples can be assigned to the diffraction planes of (220), (400) and (440) of spinel $NiAl_2O_4$, respectively. The peak intensity of the $NiAl_2O_4$ phase increased with the increase in Al_2O_3 content in the anodes. This result strongly suggests that the nickel in the anode reacted with the Al_2O_3 to form the $NiAl_2O_4$ spinel phase in the Al_2O_3-modified anodes. For the SnO_2-incorporated anode, SnO_2 and Y_2SnO_7 phases were detected. The various anodes were then reduced at 850 °C in a hydrogen atmosphere for 1 h; the XRD results are shown in Fig. 1b. Both the $NiAl_2O_4$ and NiO phases disappeared for the two alumina-containing anodes while the Al_2O_3 and Ni phases were detected instead, suggesting that the $NiAl_2O_4$ spinel structure was fully reduced under the hydrogen atmosphere. For the SnO_2-incorporated anode, the SnO_2 and Y_2SnO_7 phases were still detected along with the Ni and YSZ phases, which could not be reduced by hydrogen even at 850 °C.

Considering that the anode performance could be highly affected by its microstructure, the electrode morphologies of the various reduced anodes were also examined by SEM; typical SEM images are shown in Fig. S1. It was found that the addition of the oxide modifiers reduced the anode particle size compared to the pristine anode, whereas alumina was more effective than tin oxide for such reduction. For example, the average particle sizes of Ni–YSZ, Ni–YSZ–2.68Sn, Ni–YSZ–2.68Al and Ni–YSZ–10Al were around 1.3 μm, 650 nm, 400 nm and 410 nm, respectively. To further confirm the reduced particle sizes after the introduction of the Al_2O_3 and SnO_2 additives, the anode materials were examined by TEM; typical TEM images are shown in Fig. 2. The Ni–YSZ sample had an average size of 1.5–2 μm for the primary particles, whereas the Ni–YSZ–2.68Sn showed much smaller particles with sizes of approximately 700 nm. The two alumina-promoted anodes had even smaller particle sizes of approximately 400 nm. HR-TEM images for the Ni–YSZ sample, as shown in Fig. S2a, exhibited two fringes with distances of 0.257 and 0.202 nm, which matched with the spacing of the (202) diffraction plane of YSZ oxide and the

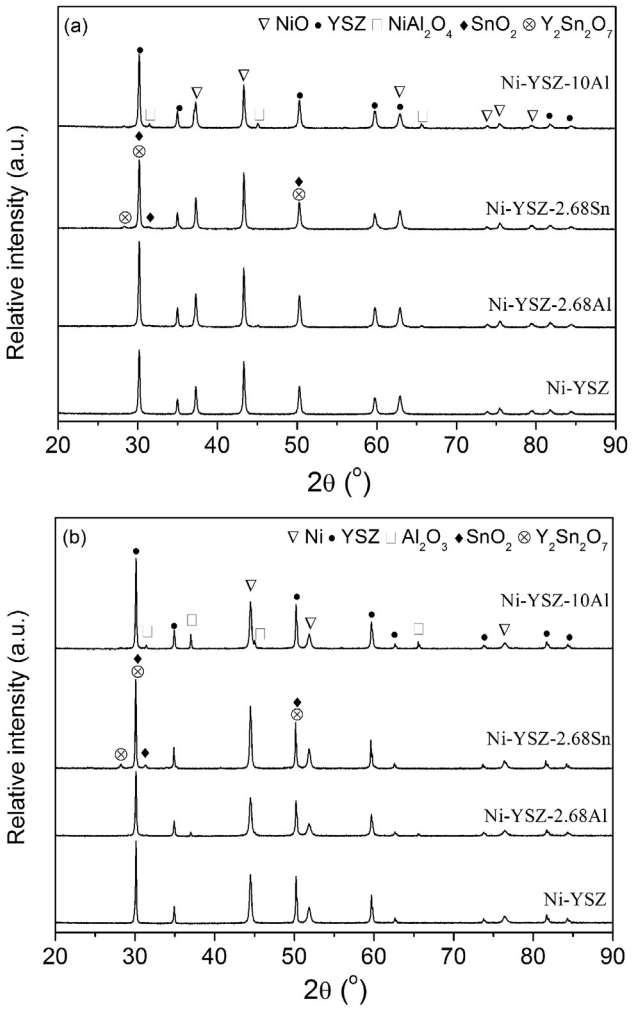

Fig. 1. XRD patterns of the various unreduced (a) and reduced (b) anodes.

(111) diffraction plane of Ni, respectively. In addition to the two main phases, a SnO_2 phase with a fringe distance of 0.213 nm, assignable to the fringe distance for the (112) plane, was also observed in the Ni–YSZ–2.68Sn sample and an alumina phase with a fringe distance of 0.195 nm assigned to the (207) diffraction plane was observed in the two alumina-containing samples, as shown in Fig. S2b–d.

In addition to the microstructure, electrical conductivity is another important parameter that can affect the performance of the anode of SOFCs. The anode cermets were generally prepared by mixing NiO and YSZ powders and then reducing the NiO phase to nickel metal at high temperature in a reducing gas atmosphere, typically hydrogen. After the reduction, nickel formed a percolate phase to introduce an electrical conduction pathway. However, the unreduced Al_2O_3 and SnO_2 additives may have disturbed the electron transport within the electrode. Fig. S3 presents the electrical conductivity of the various reduced samples as a function of temperature under a H_2–Ar atmosphere. Indeed, a reduction in the electrical conductivity was observed for the anode material after the addition of the oxide additives. A small amount of alumina did not cause a sharp decrease in the conductivity compared to that of the pristine Ni–YSZ anode (1609 versus 1945 S cm^{-1} at 800 °C). However, Ni–YSZ–2.68Al had a higher conductivity value than that of Ni–YSZ–2.68Sn at all the investigated temperatures; for example, the values were 1609 and 1334 S cm^{-1} for the

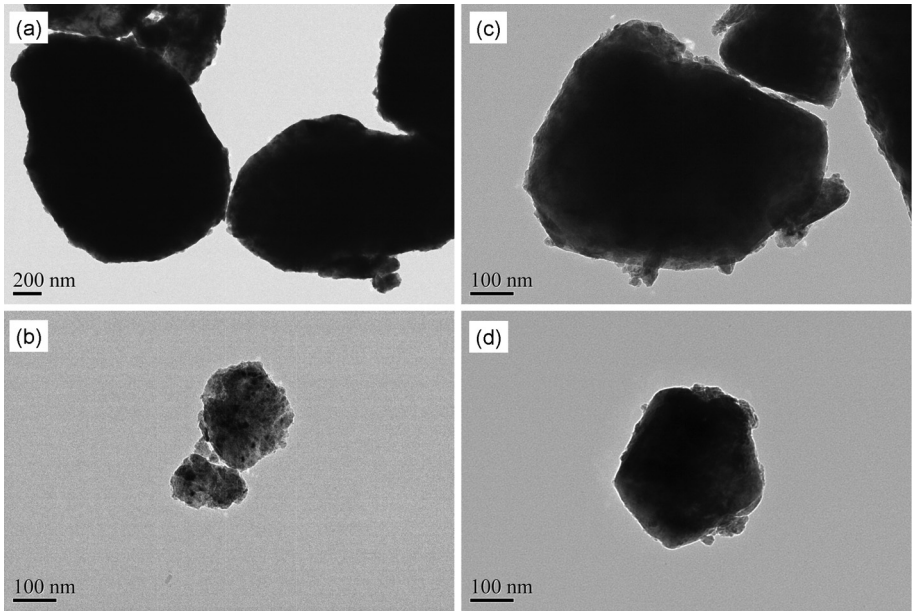

Fig. 2. TEM images of the various anodes. Ni–YSZ (a), Ni–YSZ–2.68Al (b), Ni–YSZ–2.68Sn (c), Ni–YSZ–10Al (d).

Ni–YSZ–2.68Al and Ni–YSZ–2.68Sn at 800 °C, respectively. Conversely, the addition of excess alumina could sharply decrease the electrical conductivity due to the formation of a large amount of $NiAl_2O_4$, and the conductivity for the Ni–YSZ–10Al anode was reduced to only 1018 S cm^{-1} at 800 °C. Thus, the alumina content in the anode should be well tailored to minimize the effect on electrical conductivity.

3.2. Catalytic activity and carbon deposition

The catalytic performance of the various anodes for the conversion of biogas (CO_2 reforming of methane) to syngas was investigated at atmospheric pressure and temperatures in the range of 550–850 °C. It was found that the main products were H_2 and CO, while only minor quantities of byproducts, such as H_2O, were formed based on the analysis of the gas chromatograph (Varian 3800). As shown in Fig. 3, the four anodes all showed good catalytic activity for methane conversion above 800 °C due to the effect of thermodynamics, but they were considerably diversified in catalytic activity at lower operation temperatures when the kinetics became the driving force rather than thermodynamics. For example, a methane conversion of 62.8% was obtained for the pristine Ni–YSZ anode at 650 °C, while it was only 56.4% for Ni–YSZ–2.68Sn. Such a difference may be explained by the reduced active sites after the SnO_2 addition [23]. Interestingly, the two alumina-modified anodes had a much higher methane conversion. Both reached a methane conversion above 80% at 650 °C. Similar trends for CO_2 conversion of the four anode materials were also observed; the results are shown in Fig. 3b. The two alumina-promoted anodes had a much higher CO_2 conversion than the Ni–YSZ and Ni–YSZ–2.68Sn anodes at the investigated temperatures.

The operational stability of the SOFCs operating on hydrocarbon fuels is closely related to the coke formation on the anodes. We employed O_2-TPO to characterize the coking behavior of the various anodes; the results are shown in Fig. 4. The CO_2 peak areas reflected the amount of carbon deposited on the anodes, which were calculated as 3.55×10^{-6}, 2.37×10^{-6}, 1.06×10^{-6} and 1.19×10^{-6} for the Ni–YSZ, Ni–YSZ–2.68Sn, Ni–YSZ–2.68Al and Ni–YSZ–10Al samples, respectively. This result demonstrates that the addition of oxide promoters increased the coking resistance of the cermet anodes and that Ni–YSZ–2.68Al exhibited the best coking resistance. However, the excess alumina had a negative effect on the coking resistance, which may be explained by the fact that a large amount of alumina increased the surface acidity of the anodes.

3.3. Cell performance

The impact of the Al_2O_3/SnO_2 additives on cell performance was first evaluated by operating on hydrogen fuel. Table 1 displays the peak power densities (PPDs) of the fuel cells with the various anodes operating on hydrogen at different temperatures. PPDs of 667, 665, 495 and 572 mW cm^{-2} were achieved at 850 °C for the fuel cells with the Ni–YSZ, Ni–YSZ–2.68Al, Ni–YSZ–2.68Sn and Ni–YSZ–10Al anodes, respectively. By applying hydrogen fuel, the cell performance was mainly determined by the electrical conductivity properties of the electrodes, while the catalytic activity for methane conversion and coking resistance is not important. The different power outputs for the fuel cells with the Ni–YSZ, Ni–YSZ–2.68Al and Ni–YSZ–10Al anodes operating on hydrogen fuel may be explained by the difference in electronic conductivity of the three anodes, while the relatively poor performance of the cell with the Ni–YSZ–2.68Sn anode may be attributed to the reduced active sites for hydrogen electrocatalytic oxidation after the introduction of tin oxide, as demonstrated in the literature [23].

Fig. 5a presents the corresponding *I–V* and *I–P* polarization curves of the fuel cells with various anodes operating on simulated biogas at 800 °C. PPDs of 424, 478, 272 and 408 mW cm^{-2} were achieved at 800 °C for the fuel cells with the Ni–YSZ, Ni–YSZ–2.68Al, Ni–YSZ–2.68Sn and Ni–YSZ–10Al anodes operating on simulated biogas, respectively. The fuel cell with the Ni–YSZ–2.68Al anode demonstrated the best power output among the four cells. Based on previous catalytic results, the performance of the other two cells without alumina addition was likely limited by the insufficient catalytic activity for the methane conversion to syngas. In fact, at reduced temperatures, similar power output was achieved for the fuel cell with the Ni–YSZ–2.68Al anode operating on biogas fuel and hydrogen

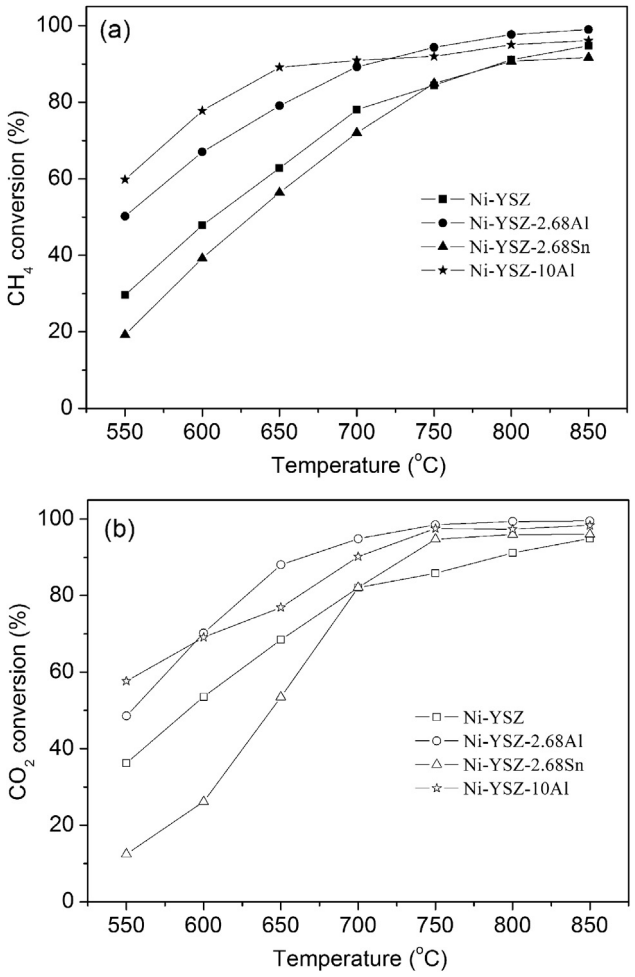

Fig. 3. Catalytic activity of the various anodes for CO_2 reforming of methane in biogas. Methane conversion (a), CO_2 conversion (b).

fuel, which could be attributed to the high catalytic activity of the Ni–YSZ–2.68Al anode for CO_2 reforming of methane, as demonstrated in Fig. 3. The area-specific resistances of the fuel cells were determined from the impedance spectra as shown in Fig. 5b. In EIS, the high-frequency offset on the real axis is primarily a result of the resistance of the electrolyte, whereas

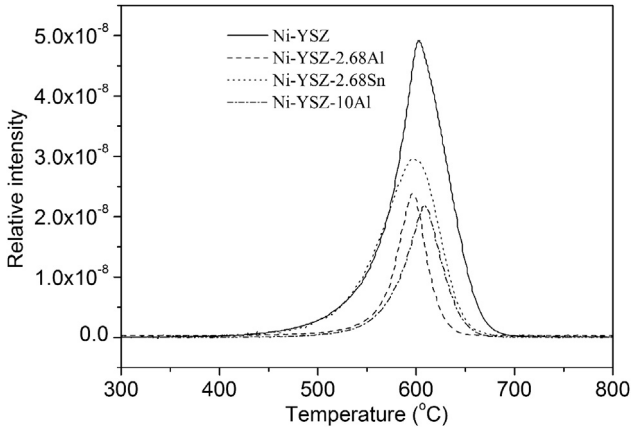

Fig. 4. Carbon deposition behaviors of the various anodes after treatment in biogas for 30 min at 750 °C.

Table 1
PPDs for the fuel cells with various anodes operating on hydrogen and biogas at different temperatures.

Anodes	Fuels	PPDs at different temperatures (mW cm^{-2})			
		850 °C	800 °C	750 °C	700 °C
Ni–YSZ	H_2	667	524	373	261
	Biogas	520	424	278	168
Ni–YSZ–2.68Al	H_2	665	514	372	241
	Biogas	571	478	350	247
Ni–YSZ–2.68Sn	H_2	495	360	233	123
	Biogas	409	272	147	84
Ni–YSZ–10Al	H_2	572	454	331	235
	Biogas	519	408	301	214

the difference between the high and low frequency intercepts on the real axis is associated with the electrode contribution, which includes both the anode and the cathode. As shown in this figure, the fuel cell with Ni–YSZ–2.68Al anode showed the lowest electrode polarization resistance and the fuel cell with Ni–YSZ–2.68Sn anode presented the largest one, which was in good agreement with the *I–V* and *I–P* results. Therefore, Ni–YSZ–2.68Al could be a highly active and coking-resistant anode material for SOFCs operating on biogas.

3.4. Operational stability

To determine the effect of oxide additives on cell operational stability, which is crucial for practical applications, three similar

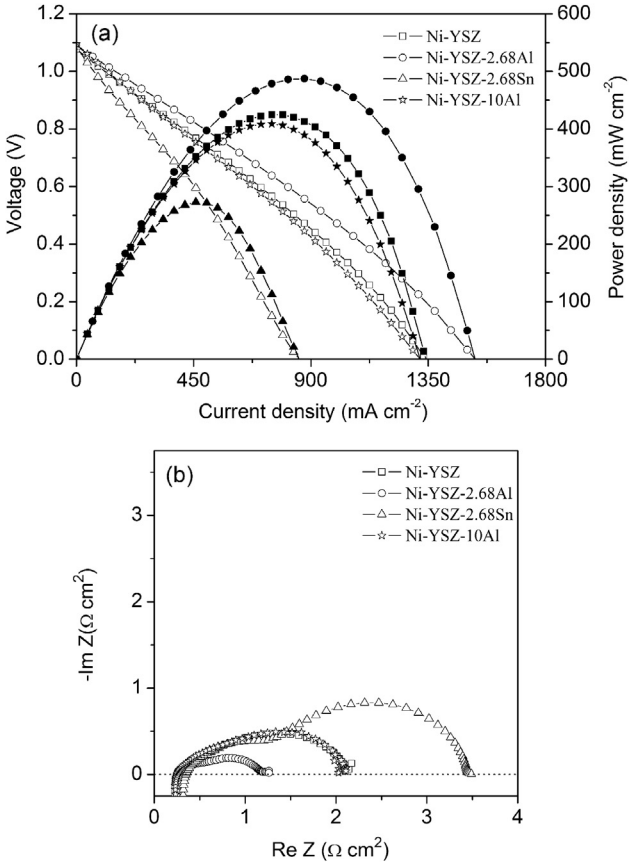

Fig. 5. *I–V*, *I–P* curves (a) and impedance spectra (b) for the fuel cells with various anodes operating on biogas at 800 °C.

fuel cells were first polarized under a constant current density of 200 mA cm^{-2} for 24 h at 750 °C by operating on hydrogen fuel to obtain a stable performance; then, the stability tests were conducted by operating on simulated biogas. Fig. 6 shows the time dependence of the voltage under a current density of 200 mA cm^{-2}. For the cell with the pristine Ni–YSZ anode, the voltage decreased progressively, and the cell eventually failed after 35 h of operation. In contrast, the addition of oxide additives could improve the operational stability of the fuel cells. For example, the performance of the cell with the Ni–YSZ–2.68Sn anode was relatively stable for a period of 40 h, but the fuel cell still failed after operating for 75 h. In contrast, the fuel cell with the Ni–YSZ–2.68Al anode operated for 130 h without any noticeable decay in performance. As shown in Fig. 6, a straight line using linear regression was use to fit the voltage–time data, and the decay rates are 663, 410 and 31.8 mV/100 h for Ni–YSZ, Ni–YSZ–2.68Sn and Ni–YSZ–2.68Al anodes. This significant improvement in the operational stability is clearly due to the suppressed coke formation after the introduction of alumina into the Ni–YSZ anodes.

Carbon deposition over the various anodes after the stability test was studied by XRD as shown in Fig. 7. As can be seen, Ni–YSZ and Ni–YSZ–2.68Sn anodes had a C peak while there was no obvious diffraction peak assign to the C peak in the XRD pattern of Ni–YSZ–2.68Al anode, suggesting more serious coke formation on the Ni–YSZ and Ni–YSZ–2.68Sn anodes as compared with Ni–YSZ–2.68Al anode. Carbon deposition over the various anodes after the stability test was also investigated by SEM–EDX at selected regions, as shown in Fig. S4, including two regions: the YSZ electrolyte for region 1, the anode layer near the anode–electrolyte interface for region 2. Specifically, region 2 is approximately 20 μm from the anode–electrolyte interface. The freshly cracked YSZ electrolyte was used to eliminate the effect of contaminated carbon during the preparation process on the EDX results. The carbon content of region 1 for all three cells was approximately 5 wt.%, suggesting the uniform contamination of carbon in the preparation process. It is well known that the electro-active zone of the anode layer is typically less than 20 μm in thickness nearest to the electrolyte layer [26]. Carbon deposition over this region would result in reduced active sites for the electrochemical oxidation of the fuel, resulting in serious deterioration of the cell performance and the introduction of large internal stress. As shown in Fig. S4, the carbon contents in region 2 are 14, 11 and 6 wt.% for the Ni–YSZ, Ni–YSZ–2.68Sn, and Ni–YSZ–2.68Al anodes, respectively. It is

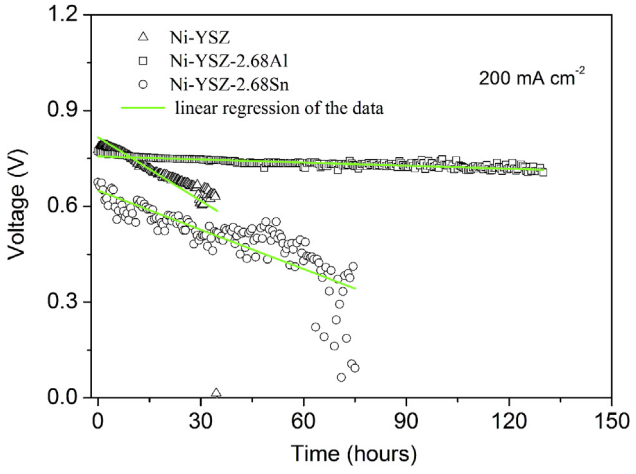

Fig. 6. The time dependence of the voltage under a specific current density of 200 mA cm^{-2} at 750 °C of the fuel cells with various anodes.

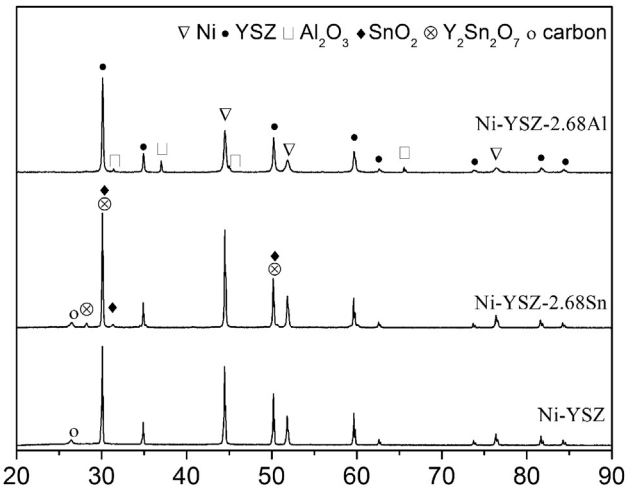

Fig. 7. XRD patterns of the various anodes after the stability test.

suggested that there is almost no coke formation in region 2 of the fuel cell with the Ni–YSZ–2.68Al anode, which could account for the good operational stability. All the above results suggest that the alumina-modified Ni–YSZ could be used as highly active and coking-resistant anode materials for SOFCs on biogas with improved power output and operational stability.

4. Conclusions

To enhance the catalytic activity of anode materials for the internal reforming of hydrocarbon-based gases such as biogas, alumina and tin oxides were selected to modify traditional Ni–YSZ anodes. It was found that the addition of the modifier could reduce the particle sizes and increase the coking resistance of the Ni–YSZ anode, as evidenced by SEM, TEM and O_2-TPO. The incorporation of a suitable amount of alumina could improve the power output of the SOFCs operating on biogas. However, tin oxide and excessive alumina had a negative effect on the cell performance, which was mainly attributed to the low catalytic activity for CO_2 reforming of methane and low electronic conductivity, respectively. The fuel cell with the appropriate amount of alumina-modified anodes delivered a stable operation on biogas of approximately 130 h at 750 °C, while the unmodified Ni–YSZ anode and tin oxide-modified Ni–YSZ anode failed after 35 and 75 h of operation at the same conditions, respectively. The low cost of alumina, easy preparation, excellent catalytic activity, high coking resistance and good operational stability indicate that alumina-promoted Ni–YSZ is promising for application as an anode material for SOFCs operating on biogas. In the future, we will focus on the study of the effects of weight percents of aluminum oxide and incorporation methods on the catalytic activity, coking resistance and electrochemical performance of aluminum oxide modified Ni-based anode.

Acknowledgments

This work was supported by the “National Science Foundation for Distinguished Young Scholars of China” under contract No. 51025209 and the Doctoral Fund of Ministry of Education of China (20113221110002).

Appendix A. Supplementary data

Supplementary data related to this article can be found at http://dx.doi.org/10.1016/j.jpowsour.2014.06.087.

References

[1] S. Park, J.M. Vohs, R.J. Gorte, Nature 404 (2000) 265–267.
[2] T. Hibino, A. Hashimoto, T. Inoue, J. Tokuno, S. Yoshida, M. Sano, Science 288 (2000) 2031–2033.
[3] Z.P. Shao, S.M. Haile, J. Ahn, P.D. Ronney, Z.L. Zhan, S.A. Barnett, Nature 435 (2005) 795–798.
[4] Z.L. Zhan, S.A. Barnett, Science 308 (2005) 844–847.
[5] W. Wang, C. Su, Y.Z. Wu, R. Ran, Z.P. Shao, Chem. Rev. 113 (2013) 8104–8151.
[6] N.Z. Muradova, T.N. Veziroğlu, Int. J. Hydrogen Energy 33 (2008) 6804–6839.
[7] A. Kumar, D.D. Jones, M.A. Hanna, Energies 2 (2009) 556–581.
[8] J. Van herle, F. Maréchal, S. Leuenberger, Y. Membrez, O. Bucheli, D. Favrat, J. Power Sources 131 (2004) 127–141.
[9] G. Goula, V. Kiousis, L. Nalbandian, I.V. Yentekakis, Solid State Ionics 177 (2006) 2119–2123.
[10] H. He, J.M. Hill, Appl. Catal. A 317 (2007) 284–292.
[11] Y. Shiratori, T. Ijichi, T. Oshima, K. Sasaki, Int. J. Hydrogen Energy 35 (2010) 7905–7912.
[12] J. Staniforth, K. Kendall, J. Power Sources 86 (2000) 401–403.
[13] Y. Shiratori, T. Oshima, K. Sasaki, Int. J. Hydrogen Energy 33 (2008) 6316–6321.
[14] A. Lanzini, P. Leone, Int. J. Hydrogen Energy 35 (2010) 2463–2476.
[15] S.W. Tao, J.T.S. Irvine, Nat. Mater. 2 (2003) 320–323.
[16] S. McIntosh, J.M. Vohs, R.J. Gorte, J. Electrochem. Soc. 150 (2003) A470–A476.
[17] L. Yang, Y. Choi, W. Qin, H. Chen, K. Blinn, M. Liu, P. Liu, J. Bai, T.A. Tyson, M. Liu, Nat. Commun. 2 (2011) 357.
[18] A. Yan, M. Phongaksorn, D. Nativel, E. Croiset, J. Power Sources 210 (2012) 374–380.
[19] M. Asamoto, S. Miyake, K. Sugihara, H. Yahiro, Electrochem. Commun. 11 (2009) 1508–1511.
[20] Y. Shiratori, Y. Teraoka, K. Sasaki, Solid State Ionics 177 (2006) 1371–1380.
[21] Himeko Orui, Reiichi Chiba, Kazuhiko Nozawa, Hajime Arai, Ryoji Kanno, J. Power Sources 238 (2013) 74–80.
[22] H. Kan, H. Lee, Appl. Catal. B 97 (2010) 108–114.
[23] A. Singh, J.M. Hill, J. Power Sources 214 (2012) 185–194.
[24] H.X. Gu, R. Ran, W. Zhou, Z.P. Shao, J. Power Sources 172 (2007) 704–712.
[25] W. Wang, C. Su, R. Ran, H.J. Park, C. Kwak, Z.P. Shao, Int. J. Hydrogen Energy 36 (2011) 5632–5643.
[26] S.X. Liu, W. Kong, Z.J. Lin, Energies 2 (2009) 427–444.